



ARTICLE

Research on the Performance of Titanium Gypsum Concrete Based on Calcium-Silicon-Sulfur Ratio

Lixia Guo^{1,2,3}, Weikai Wang¹, Ling Zhong^{1,2,3,*} and Yuhang Guo¹

¹School of Water Conservancy, North China University of Water Resources and Electric Power, Zhengzhou, 450046, China

²Henan Water Valley Research Institute, Zhengzhou, 450046, China

³Henan Key Laboratory of Water Environment Simulation and Treatment, Zhengzhou, 450002, China

*Corresponding Author: Ling Zhong. Email: Zhonling@ncwu.edu.cn

Received: 01 April 2022 Accepted: 20 May 2022

ABSTRACT

Based on the high sulfur content in titanium gypsum, the concept of the calcium-silicon-sulfur (Ca/Si/S) ratio was proposed. The Ca/Si/S ratio of concrete was adjusted by changing the titanium gypsum, fly ash, and cement content. The effects of different Ca/Si/S ratios on the mechanical properties, hydration products, and concrete microstructure were investigated by nuclear magnetic resonance, uniaxial compression, and scanning electron microscopy. The result shows: (1) The compressive strength of concrete mixed with titanium gypsum increases first and then decreases with the Ca/Si/S ratio decrease. When the Ca/Si/S ratio is 1:0.85:0.10, the strength reaches the peak and is lower than the blank group. (2) The microstructure indicates the addition of titanium gypsum can effectively stimulate the activity of fly ash. Still, too much or too little titanium gypsum will hamper concrete strength development. (3) Titanium gypsum concrete's nuclear magnetic resonance T2 spectrum has two characteristic peaks. With the Ca/Si/S ratio decreasing, the micropores in the concrete expand towards the macropores. The compressive strength is negatively correlated with the proportion of macropores and is positively correlated with the proportion of no-capillary pores.

KEYWORDS

Titanium gypsum; calcium-silicon-sulfur ratio; compressive strength; pore structure

Nomenclature

TG	Titanium gypsum
TGC	Titanium gypsum concrete
Ca/Si/S	Calcium-silicon-sulfur ratio
SEM	Scanning electron microscopy
EDS	Energy dispersive spectroscopy
NMR	Nuclear magnetic resonance
SACM	Sulfoaluminate cementitious materials



1 Introduction

Titanium gypsum (TG) is a solid waste [1,2] with dihydrate gypsum ($\text{CaSO}_4 \cdot 2\text{H}_2\text{O}$) as the main component, which is produced by adding lime or calcium carbide slag to neutralize acidic wastewater during the preparation of titanium dioxide using the sulfuric acid method. It is difficult to recycle because of its high free water content, impurity content, and poor mechanical properties [3]. According to statistics, the annual emission of TG in China is as high as 30 million tons, which occupies land resources and causes a significant impact on the environment [4,5]. These enterprises are under considerable pressure to go green, increasing their burdens, which must be settled urgently.

Under China's "dual carbon" background, harmless treatment, resource utilization, and industrial development [6–8] are the best approaches to industrial solid waste. For example, Chen et al. [9] studied the feasibility of using industrial by-products (fly ash and slag) and aquaculture waste (crushed waste oyster shells) to replace cement and fine aggregate to prepare environmentally friendly mortar through experiments. The results showed that crushed waste oyster shells replaced 30% of the fine aggregate, and 30% of the cement was replaced by fly ash and ground granulated blast-furnace slag to obtain the mortar with the best performance. Li et al. [10] studied the feasibility of industrial solid wastes (fly ash, desulfurization gypsum, steel slag) as mineral filler materials through experiments, which solved the environmental risks caused by industrial solid waste and reduced the cost of cement-based cementitious materials. Ju et al. [11] proposed a precipitation-solvent extraction-leaching process, which can effectively separate and recover titanium, scandium, and iron in acidic wastewater and realize the resource utilization of red gypsum. Some scholars have done a lot of research to solve the damage of solid waste TG to the environment and realize the comprehensive utilization of solid waste resources. Li et al. [12] used titanium gypsum with high impurities and heavy metals content to synergize with three solid wastes (Carbide slag, Aluminum dust and Caol Gangue) to prepare sulfoaluminate cementitious materials (SACM). It was found that the solid waste-based SACM can effectively solidify heavy metals contained in raw materials such as titanium gypsum during the hydration process. Titanium gypsum is also a potential and effective soil conditioner that can effectively fix heavy metals in soil, thereby improving the growth of crops [13,14]. Da et al. [15] discussed the feasibility of mixing titanium-containing pickling sludge into cement raw material to produce cement through experiments. They found that when the titanium-containing pickling sludge content is 1%, the cement's workability was the best at different calcination temperatures. The unconfined compressive strength of the produced mortar is up to 49.37 MPa (28 d). Yessengaziyev et al. [16] analyzed TG's physical and chemical results in extracting titanium dioxide and calcium nitrat. They found that titanium mainly exists in the form of low-grade titanium oxide, hydrated titanium oxide, and aluminum titanium niobium oxide. Gazquez et al. [17,18] investigated the primary mechanical, elastic, and thermodynamic properties of cement made with different proportions of TG, an industrial waste from titanium dioxide. The results showed that TG could replace natural gypsum for cement production without reducing the cement quality.

In addition, many studies on titanium gypsum-based composite cementitious materials have indicated a perspective of actual feasibility in construction and building. Zhang et al. [19,20] used TG to prepare mortar. When the content of TG was increased from 10% to 40%, the results of X-ray diffraction and topography analysis showed that the interwoven hydrates in the hardened mortar were acicular ettringite, unreacted bar-like gypsum, and filamentous C-(A)-S-H, ensuring the mortar with good water resistance. A cost-effective method is provided for producing high-strength cementitious materials using TG and titanium slag to replace ordinary Portland cement. In addition, titanium gypsum, titanium residues, and Portland cement are used to prepare TG foamed concrete. The hydrating dynamics, mechanical properties, and microstructures of TG foamed concrete are studied. The results indicated that ordinary Portland cement: titanium residue: titanium gypsum = 10:45:45 (quality ratio), and add 2% lime, 4% sulfuric acid saline cement, 0.4% Na_2SO_4 , 0.2% water reducer, 4.6% foam can make high-performance foamed concrete. Cai

et al. [21] studied the feasibility of using red gypsum (RG) as a substitute for fly ash to prepare autoclaved aerated concrete (AAC) and found that the best red gypsum replacement rate in AAC was 20%. Zhang et al. [22] calcined TG as raw material to produce gypsum blocks and studied the effects of cement, water-solid ratio, water reducing agent, citric acid content, and hydration age on gypsum blocks. The optimum water-cement ratio, cement dosage, and water reducing agent dosage were obtained as 0.9%, 10%, and 2 wt%, respectively. Hughes et al. [23] used TG, blast furnace slag, and a small amount of lime to make TG-based adhesive. The study indicated that TG-based adhesives have higher strength and stiffness and are better than Portland cement, suggesting the potential to integrate TG into concrete block mixes. And found that the cost of TG-based adhesive is lower and has an obvious price advantage. Although there are many measures for the comprehensive utilization of TG, they are all in the research and exploration stage, and almost no one has been used for industrial production.

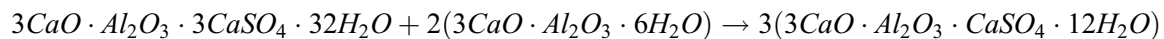
To maximize the utilization of TG more effectively, in this study, TG was used as a sulfur raw material to prepare concrete. This paper also investigates the impact of the calcium-silicon-sulfur (Ca/Si/S) ratio on concrete's compressive strength, pore structure, and microscopic morphology by adjusting the relative content of raw materials.

2 Ca/Si/S Ratio

The main minerals of Portland cement clinker were tricalcium silicate ($3\text{CaO}\cdot\text{SiO}_2$), dicalcium silicate ($2\text{CaO}\cdot\text{SiO}_2$), tricalcium aluminate ($3\text{CaO}\cdot\text{Al}_2\text{O}_3$), and tetracalcium aluminoferrite ($4\text{CaO}\cdot\text{Al}_2\text{O}_3\cdot\text{Fe}_2\text{O}_3$). Cement and admixtures (TG, fly ash) were mixed and hydrated. Tricalcium aluminate had the highest activity and reacted with dihydrate gypsum ($\text{CaSO}_4\cdot 2\text{H}_2\text{O}$), the main component of TG, to form high-sulfur calcium sulfoaluminate hydrates, namely ettringite (AFt) [24,25]. The hydration equation is as follows:



If the TG is insufficient, part of the ettringite will be converted into monosulfur calcium sulfoaluminate hydrates (AFm), namely:



To sum up, acicular ettringite crystals are formed first during the cement hydration, and monosulfur calcium sulfoaluminate hydrates may also be generated when the TG is insufficient. Ettringite crystals or gel-like ettringite can significantly increase the solid phase volume after absorbing water. An appropriate amount of ettringite can compensate for the shrinkage stress of concrete [26,27]. The calcium sulfoaluminate hydrate is an acicular crystal that is insoluble in water. It adheres to the surface of cement particles to prevent water absorption, thereby delaying hydration.

In addition to the above typical reactions, tricalcium silicate and dicalcium silicate are hydrated to form calcium silicate hydrate gel (C-S-H) and calcium hydroxide ($\text{Ca}(\text{OH})_2$).



where x represents the molar ratio of CaO to SiO_2 , abbreviated as the calcium-silicon ratio (C/S); n represents the amount of bound water; y represents the number of water molecules used for calcium silicate hydration.

In the equation, C-S-H was a rough approximation, and its composition varied under different concentrations of calcium hydroxide solution and temperatures. When the calcium oxide concentration in the solution was within 0.11–1.12 g/l, calcium silicate hydrates with a C/S ratio of 0.8–1.5 would be generated. When the calcium oxide concentration in the solution was greater than 1.12 g/l, calcium silicate hydrates with a C/S ratio of 1.5–2.0 would be generated.

Given the addition of TG, this paper proposes the concept of calcium-sulfur ratio, namely the molar ratio of Ca to S in high-sulfur calcium sulfoaluminate hydrates and monosulfur calcium sulfoaluminate hydrates, based on the concept of calcium-silicon ratio. The Ca/S ratio was about 2:1 or 4:1, providing a basis for mix proportion design in this experiment.

3 Equations and Mathematical Expressions

3.1 Raw Materials

In this experiment, the cement used P•O 42.5 Portland cement produced by Henan Tianrui Co., Ltd. (China), with a specific surface area of 348.7 m²/kg, a density of 3,035 kg/m³, and a 3/28 d compressive strength of 25.9/49.6 MPa, and its stability was up to standard. The fly ash used grade I ash provided by Henan Yulian Power Plant. The TG was provided by a titanium dioxide factory in Henan Province, and its organic matter content was 11.6 g/kg. The chemical composition of raw materials is shown in Table 1. Fig. 1 shows TG's scanning electron microscopy/energy dispersive spectroscopy (SEM/EDS) image. It can be seen from the figure that the TG raw materials are mainly elongated or flattened CaSO₄ crystals, to the surface of which some flocculent fine particles or agglomerates are attached, namely Fe(OH)₃. The particle size distribution curve of the used cementitious material is shown in Fig. 2.

Table 1: Chemical composition of raw materials (%)

Chemical Constituents/%	CaO	Fe ₂ O ₃	SO ₃	Al ₂ O ₃	MgO	SiO ₂	K ₂ O	Na ₂ O	TiO ₂	LOI
Cement	51.27	3.65	2.46	9.25	4.98	24.13	0.79	1.95	–	3.55
Fly ash (FA)	4.64	4.92	–	27.70	1.06	56.82	2.50	1.19	–	2.17
Titanium gypsum	31.43	15.41	37.63	2.47	1.45	5.08	0.06	0.99	3.69	–

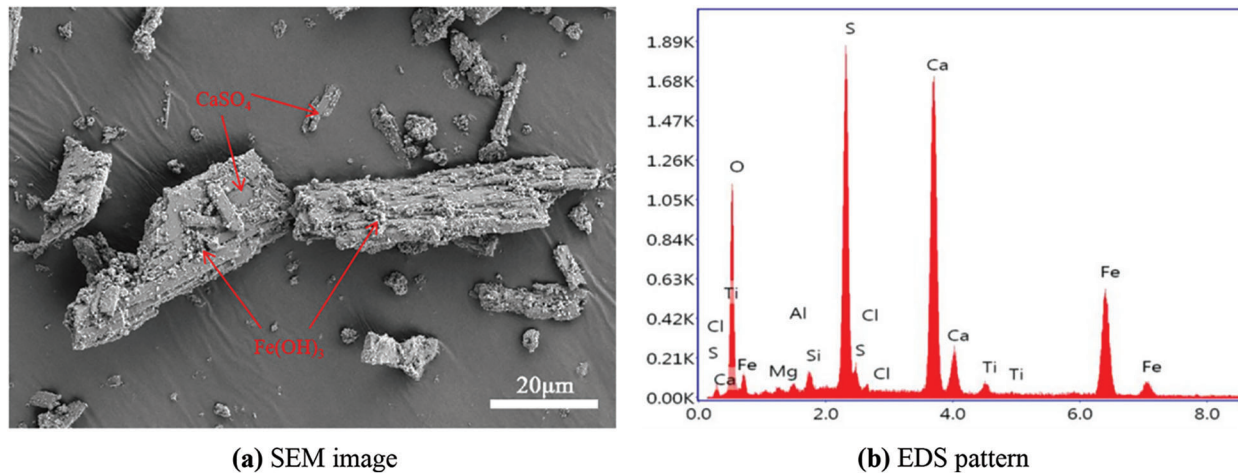


Figure 1: SEM image and EDS pattern of titanium gypsum

The fine aggregates used medium-coarse sand produced by Tanghe County Xinmiao Sand Co., Ltd. (China), with a fineness modulus of 2.94, a bulk density of 1,625.0 kg/m³, and a mud content of 1.5%.

The coarse aggregates used continuously graded crushed rocks with a 5–20 mm particle size, an apparent density of 2,720 kg/m³, a crush index of 9%, and a mud content of 0.7%. The mixing water used the laboratory tap water.

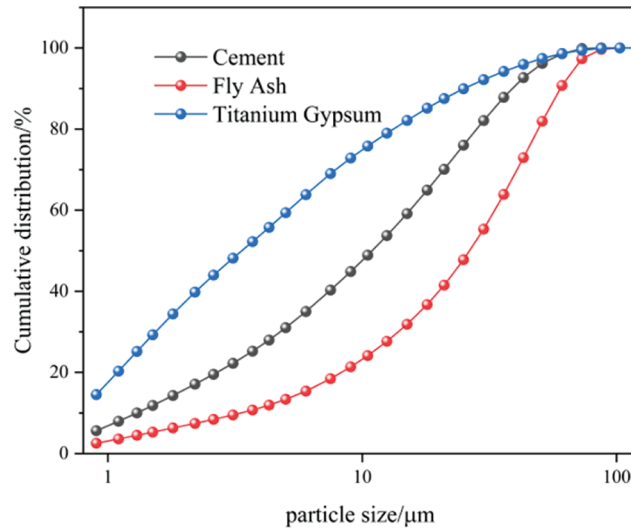


Figure 2: Particle size distribution curve of cementitious material

3.2 Design of Mix Proportion

The total quantity of cementing materials was kept unchanged based on the reference mix proportion (cementing material:sand:stone = 320:950:900), then TG was used to replace cement in the proportion of 0%, 5%, 10%, and 15%, respectively, changing the Ca/Si/S ratio, and finally, its impact on concrete properties was analyzed. The mix proportion is shown in Table 2.

Table 2: Ratio of concrete under different ratio of Ca/Si/S (kg/m³)

Sample	Cement	FA	Sand	Stone	Titanium gypsum	W/C	Ca/Si/S
T0	224	96	950	900	0	0.42	1:0.85:0.03
T5	208	96	950	900	16		1:0.85:0.07
T10	192	96	950	900	32		1:0.85:0.10
T15	176	96	950	900	48		1:0.85:0.14

The experiment used the Ca/Si/S ratio as the single-factor control variable to design the mix proportion. The percentages of effective CaO, SiO₂, and SO₃ in the raw materials are shown in Table 1. The Ca/Si/S ratio was calculated using the formula (1).

$$Ca/Si/S = A/B/C \tag{1}$$

where

$$A = (m_c \times 51.27\% + m_f \times 4.64\% + m_t \times 31.43\%) / 56$$

$$B = (m_c \times 24.13\% + m_f \times 56.82\% + m_t \times 5.08\%) / 60$$

$$C = (m_c \times 2.46\% + m_t \times 37.63\%) / 80$$

where m_c is the mass of cement, kg; m_f is the mass of fly ash, kg; m_t is the mass of TG, kg; 56 represents the molar mass of CaO; 60 represents the molar mass of SiO₂, and 80 represents the molar mass of SO₃. In the group of the TG mentioned above, cement and fly ash excluded organic matters.

3.3 Experimental Methods

By *SL/T 352-2020 Test Code for Hydraulic Concrete*, four groups of 100 mm × 100 mm × 100 mm specimens were prepared, with 12 in each group. After pouring, the specimens were placed indoors for 24 h and then demolded. The demolded specimens were transferred to a standard curing room (temperature: 20°C ± 2°C, humidity: 95%) for curing for 7 and 28 d, respectively.

A YAW-5000 electro-hydraulic servo pressure testing machine was used to test the compressive strength of the specimens. During the test, the test pieces were continuously and uniformly loaded at a speed of 0.3 MPa/s.

MesoMR12-060H-I Nuclear Magnetic Resonance Spectroscopy (NMR) equipment was used to test the pore structure of concrete. 28 d-cured specimens were placed in a vacuum environment of −0.1 MP for 24-h saturation, and then put into the coil of the NMR equipment. Their NMR relaxation was measured using the NMR analysis system. After the Carr-Purcell-Meiboom-Gill sequence attenuation signal data was collected, data inversion was performed to obtain the T2 spectrogram, which was then converted into a pore size distribution diagram. The pore size under test was between 0.1 nm and 200 μm.

Gemini-300 thermal field emission scanning electron microscope was used in the SEM test. The test samples were fragments randomly selected after the compression test. Before the SEM test, the samples were processed at about 10 mm and fixed on the sample holder with conductive adhesive for metal spraying with a 20–30 nm spray thickness. Then the Oxford X-MAX EDS was used for elemental analysis.

4 Results and Discussion

4.1 Mechanical Properties and Phase Structures of Concrete

Fig. 3 shows the relationship between the compressive strength, Ca/Si/S ratio, and titanium gypsum concrete (TGC) age. With the Ca/Si/S ratio change, the TGC compressive strength also changes and is lower than the reference group (T0). When the Ca/Si/S ratio is 1:0.85:0.10, the compressive strength of TGC at each period reaches the maximum. Compared with the reference group, the intensity at 7 d age was reduced by 47.24%, and the strength at 28 d age was reduced by 2.65%. Therefore, under these test conditions, directly adding TG to replace cement cannot maintain the original strength of concrete. With the increase of age, the compressive strength of concrete increases accordingly, but the rates are different based on the Ca/Si/S ratio. Compared with the 7d-cured specimens, the compressive strength of the 28d-cured specimens increases by 1.46, 2.51, 2.61, and 3.38 times, respectively. It can be seen that the increase in the strength of concrete mixed with TG is greater than that of the T0 group.

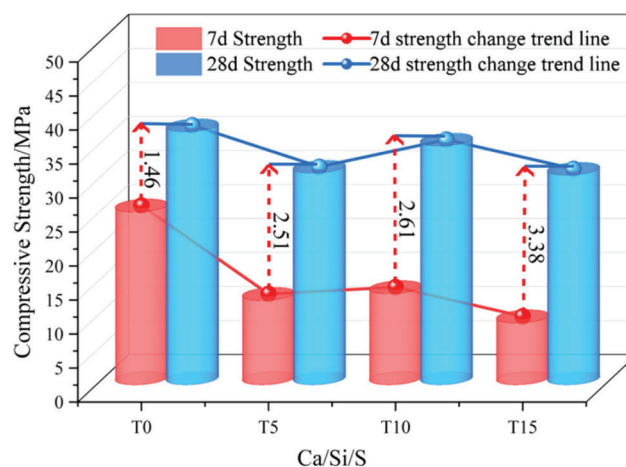


Figure 3: Compressive strength change

To clarify the mechanism of the above phenomenon, 28 d-cured concrete specimens were selected for phase analysis based on SEM images and EDS energy spectra.

Fig. 4 shows the SEM images and EDS spectra of 28 d-cured concrete specimens under different Ca/Si/S ratios. Fig. 4a is the microstructure of concrete specimens mainly composed of a small amount of C-S-H gel, $\text{Ca}(\text{OH})_2$, AFt, and non-hydrated fly ash particles, without TG. The hydration products are distributed loosely, for the addition of fly ash reduces the hydration rate of the gel. As shown in Fig. 4b, after TG is added, when the Ca/Si/S ratio is 1:0.85:0.07, the hydration products AFt and C-S-H gel gradually increase. This is because the TG participates in the hydration reaction to generate AFt, and at the same time, OH^- produced by cement hydration and SO_4^{2-} in TG stimulates the activity of fly ash [28,29]. As shown in Fig. 4c, when the Ca/Si/S ratio is 1:0.85:0.10, with the increase of TG content, the pozzolanic reaction of the fly ash is enhanced, thus generating a large number of hydration products such as AFt and C-S-H gel. These products fill the pores of the hardened paste and improve the microstructure of the cementing system. The AFt produces an expansion effect, increasing the density and strength of the gel. This is consistent with the variation mentioned above in the law of the compressive strength. As shown in Fig. 4d, when the Ca/Si/S ratio is 1:0.85:0.14, the S source in the cementing system increases due to the excessive addition of TG. When the molar ratio of Ca/Si = 1.0 [30], the remaining molar ratio of Ca and S should be 0.18/0.14. The hydration reaction of the cementitious material produces excessive AFt, which increases the expansion rate and further causes the initial damage to the internal structure of the cement, which is manifested as a decrease in strength macroscopically.

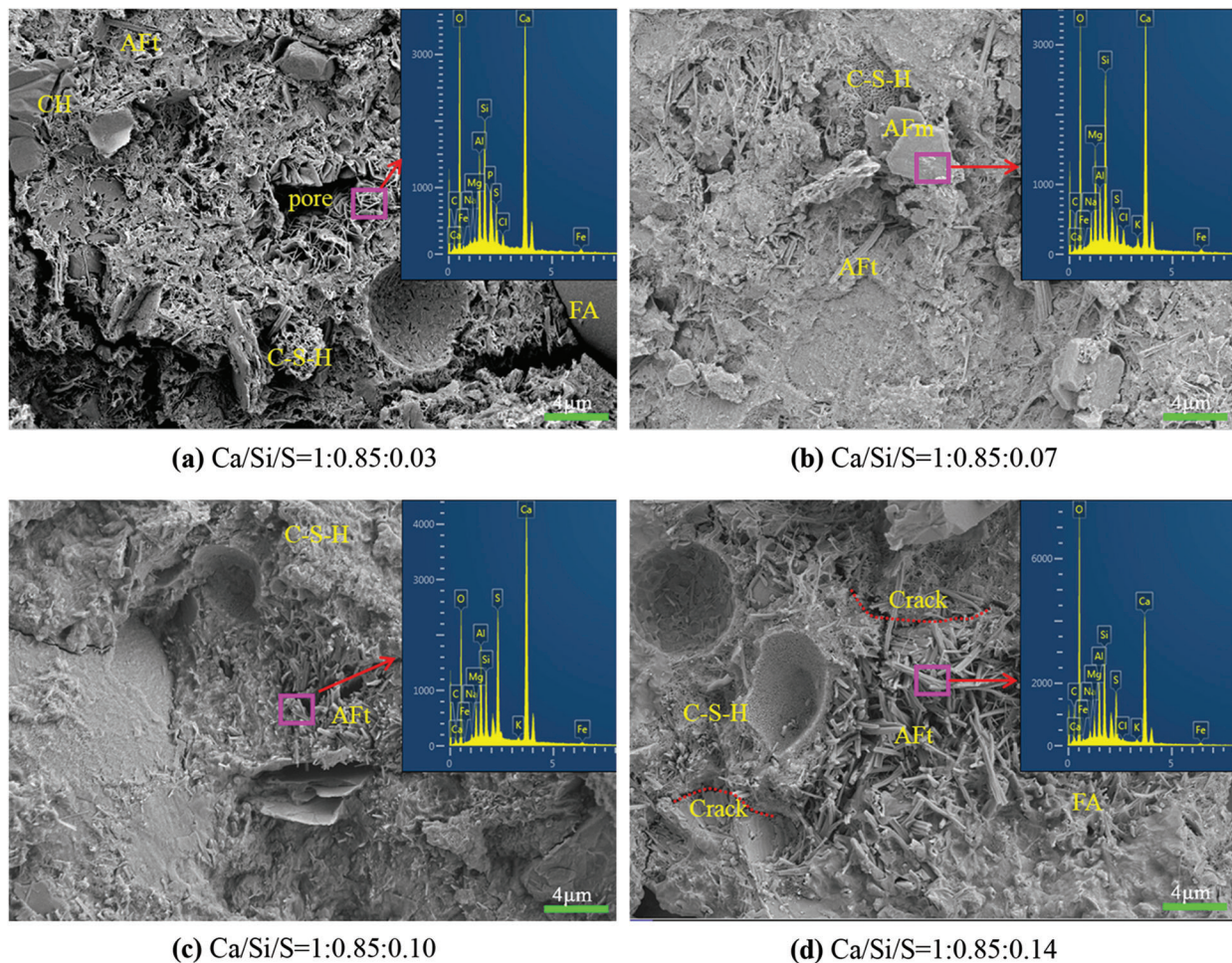


Figure 4: SEM and EDS graph of concrete

4.2 NMR-Based Pore Characteristics of TGC

According to the basic principle of NMR [31–33], the relaxation time (T_2) is directly proportional to the pore radius. The larger T_2 is, the larger the pore radius is, while the smaller the water in the pores is bound. On the contrary, the smaller T_2 is, the smaller the pore radius is, while the larger the water in the pores is bound. In the T_2 spectrogram, the peak position is related to the pore size, and the peak area determines the number of pores. The T_2 spectrum distribution curves of TGC with different Ca/Si/S ratios are shown in Fig. 5.

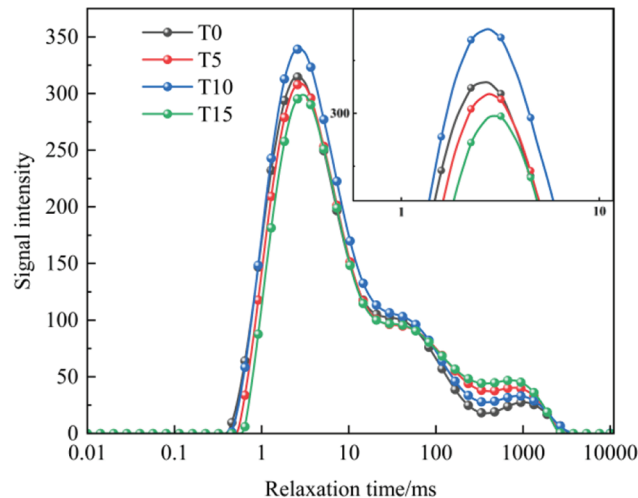


Figure 5: T_2 spectrum distribution curve of TGC

It can be seen from Fig. 5 that the NMR T_2 spectrum of concrete specimens shows two continuous peaks, and there is a big difference between the peak signals. Still, the overall characteristics of the T_2 spectrum tend to be consistent. By comparison, it was found that the first peak in the T_2 spectrum of TGC moves right with the change of the Ca/Si/S ratio, indicating that the addition of TG deteriorates the pores inside the concrete. To visually express the internal deterioration of concrete, the T_2 spectrum peak area ratio was analyzed. As shown in Fig. 6, the second peak area ratio in the test group first decreases and then increases with the Ca/Si/S ratio change. Compared with the reference group, it increases by 37%, 14%, and 67%, respectively. This is consistent with the variation law of macroscopic compressive strength, indicating a specific correlation between the proportion of macropores and the compressive strength.

To further study the effect of different pore sizes on the macroscopic properties of TGC, the pores were classified as follows. According to the relevant model proposed by I.O Butte [34], the pores of cement are divided into gel pores (<10 nm), transition pores (0.01 – 0.1 μm), and capillary pores (0.1 – 1 μm), and macropores (>1 μm). Since there are few gel pores in TGC, this paper divides gel pores and transitions pores into the non-capillary pores (0 – 0.1 μm).

It can be seen from Fig. 7 that with the decrease of the Ca/Si/S ratio, the total number of macropores increases while the total number of non-capillary pores decreases. Compared with the reference group, the total number of macropores increases by 30.3%, 8.3%, and 43.4%, respectively, while the total number of non-capillary pores decreases by 7.6%, 2.8%, and 12.6%, respectively. The change rule of the proportion of macropores and non-capillary pores is consistent with the changing trend of the compressive strength. It is mainly because the addition of TG increases the content of ettringite in the gel, and the expansion effect of ettringite leads to the deterioration of the overall pore structure. Therefore, when the Ca/Si/S ratio is 1:0.85:0.10, the TGC's pore structure is the best.

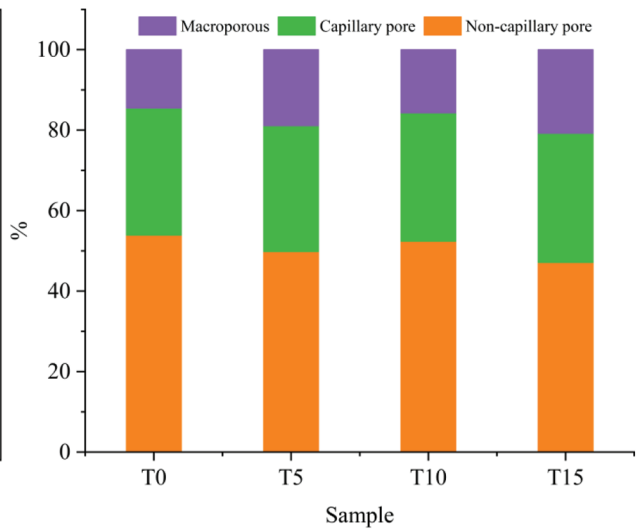
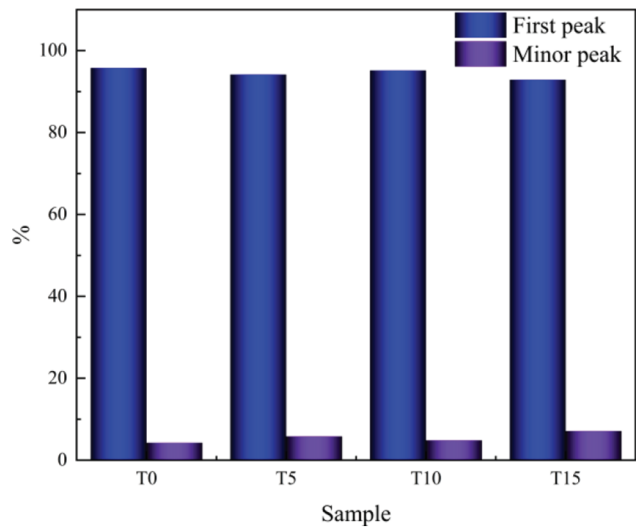
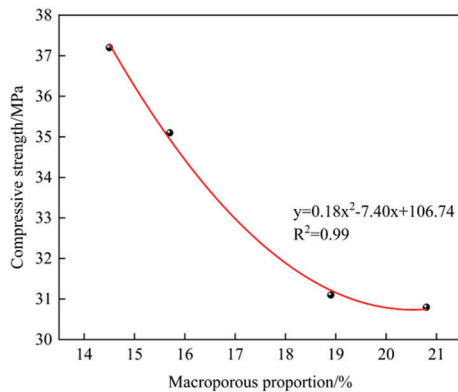
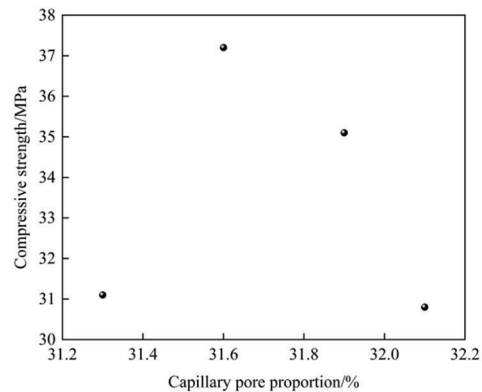


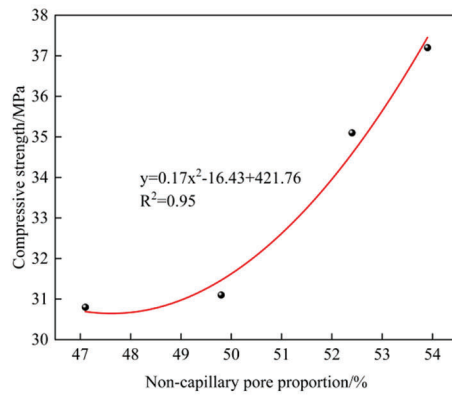
Figure 6: Ratio of peak area of T2 spectrum of TGC **Figure 7:** TGC pore type proportional distribution



(a) Compressive strength and proportion of macropores



(b) Compressive strength and proportion of capillary pores



(c) Compressive strength and proportion of non-capillary pores

Figure 8: The relationship between compressive strength and pore size distribution

5 Relationship between Compressive Strength and Pore Structure

Fig. 8 shows the relationship between TGC's compressive strength and pore size distribution. It can be seen from Fig. 8b that there is no obvious relationship between the compressive strength and the proportion of capillary pores. As seen in Figs. 8a and 8c, the compressive strength shows a negative correlation with the proportion of macropores and a positive correlation with the proportion of non-capillary pores, and the correlation coefficients (R^2) are both greater than 0.95. This result is consistent with the findings of Metha [35] and Wang et al. [36]. They found that gel pores smaller than 10 nm and transition pores within 10–100 nm are beneficial to the concrete performance, while capillary pores within 100–1,000 nm and macropores larger than 1,000 nm are detrimental to concrete performance. In summary, the proportion of macropores and non-capillary pores characterizes the macroscopic strength change of concrete.

6 Conclusion and Prospect

Through macroscopic mechanical test and microstructure analysis, the following conclusions are drawn:

1. The compressive strength of TGC is significantly subject to the Ca/Si/S ratio. The addition of TG can effectively stimulate the activity of fly ash, but too much or too little TG will hamper the development of concrete strength. When the Ca/Si/S ratio is 1:0.85:0.10, that is, when the TG content is 10%, the hydration produces a proper amount of ettringite to compensate for the shrinkage of concrete. At this time, the TGC performance is the best, but it is slightly lower than that of the reference group.
2. The T2 spectrum of TGC has two continuous peaks. With the Ca/Si/S ratio change, the non-capillary pores expand towards capillary pores, and the capillary pores expand towards macropores. TGC's compressive strength is significantly correlated with the proportion of macropores and non-capillary pores, and the correlation coefficients (R^2) are both higher than 0.95.
3. In this study, the influence of TG impurities on the hydration of composite cementitious materials was not considered. However, impurities such as Fe^{3+} , Al^{3+} , and Mg^{2+} in TG may promote the formation of crystals, increase the strength of the gel, and thus improve the resource utilization of TG. Regardless of the activity of TG, choosing an external activator to stimulate TG activity and increasing the addition of TG in concrete are also the key issues to be studied for the disposal of TG, a solid waste.

Acknowledgement: The authors acknowledgment the North China University of Water Conservancy and Hydropower for providing the test site and instruments. In addition, thanks for the joint support of the National Fund and the Innovation Project Fund of the North China University of Water Resources and Electric Power. Finally, thanks to the engineers who provided us with invaluable assistance in field and laboratory study.

Funding Statement: This work was supported by: National Natural Science Foundation of China (5210090341); Natural Science Foundation of Henan Province (202300410270); Fund of Innovative Education Program for Graduate Students at North China University of Water Resources and Electric Power, China (Grading No. YK-2021-39).

Conflicts of Interest: The authors declare that they have no conflicts of interest to report regarding the present study.

References

1. Azdarpour, A., Asadullah, M., Junin, R., Manan, M., Hamidi, H. et al. (2014). Direct carbonation of red gypsum to produce solid carbonates. *Fuel Processing Technology*, 126, 429–434. DOI 10.1016/j.fuproc.2014.05.028.

2. Kim, T. H., Tae, S. H., Chae, C. U., Choi, W. Y. (2016). The environmental impact and cost analysis of concrete mixing blast furnace slag containing titanium gypsum and sludge in South Korea. *Sustainability*, 8(6), 502. DOI 10.3390/su8060502.
3. Zha, F. S., Qiao, B. R., Kang, B., Xu, L., Chu, C. F. et al. (2021). Engineering properties of expansive soil stabilized by physically amended titanium gypsum. *Construction and Building Materials*, 303, 124456. DOI 10.1016/j.conbuildmat.2021.124456.
4. Zapata-Carbonell, J., Bégeot, C., Carry, N., Choulet, F., Delhault, P. et al. (2019). Spontaneous ecological recovery of vegetation in a red gypsum landfill: *Betula pendula* dominates after 10 years of inactivity. *Ecological Engineering*, 132, 31–40. DOI 10.1016/j.ecoleng.2019.03.013.
5. Wu, H., Feng, Y. L., Li, H. R., He, S. C., Bian, Z. Z. (2019). Red gypsum utilization and acidic wastewater treatment based on metal self-enrichment process. *Science of the Total Environment*, 691, 9–15. DOI 10.1016/j.scitotenv.2019.07.080.
6. Guo, L., Chen, P. P., Guo, L. X., Xue, Z. L., Guan, Z. et al. (2021). Pore structure characteristics of baking-free slag-sludge bricks and its correlations to mechanical properties. *Journal of Renewable Materials*, 9(10), 1805–1819. DOI 10.32604/jrm.2021.015140.
7. Zhao, Y., Chen, P., Wang, S., Ji, Y., Wang, Y. et al. (2020). Utilization of bayer red mud derived from bauxite for belite-ferroaluminate cement production. *Journal of Renewable Materials*, 8(11), 1531–1541. DOI 10.32604/jrm.2020.011462.
8. Gu, Z. H., Fang, A. G., Hua, S. D., Zhao, Q. Z., Sun, L. D. et al. (2021). Development of a soil stabilizer for road subgrade based on original phosphogypsum. *Journal of Renewable Materials*, 9(2), 253–268. DOI 10.32604/jrm.2021.011912.
9. Chen, D., Zhang, P. C., Pan, T., Liao, Y. D., Zhao, H. (2019). Evaluation of the eco-friendly crushed waste oyster shell mortars containing supplementary cementitious materials. *Journal of Cleaner Production*, 237, 1–15. DOI 10.1016/j.jclepro.2019.117811.
10. Li, J., Yilmaz, E., Cao, S. (2021). Influence of industrial solid waste as filling material on mechanical and microstructural characteristics of cementitious backfills. *Construction and Building Materials*, 299, 124288. DOI 10.1016/j.conbuildmat.2021.124288.
11. Ju, J., Feng, Y., Li, H., Wang, B. (2022). A novel approach for separation and recovery of titanium, scandium, iron from acidic wastewater and red gypsum utilization. *Mining, Metallurgy & Exploration*, 39, 1–16. DOI 10.1007/s42461-022-00600-5.
12. Li, J. W., Wang, W. L., Xu, D., Wang, X. J., Mao, Y. P. (2020). Preparation of sulfoaluminate cementitious material using harmful titanium gypsum: Material properties and heavy metal immobilization characteristics. *Waste Disposal & Sustainable Energy*, 2(2), 127–137. DOI 10.1007/s42768-020-00038-9.
13. Fauziah, I., Zauyah, S., Jamal, T. (1996). Characterization and land application of red gypsum: A waste product from the titanium dioxide industry. *Science of the Total Environment*, 188(2–3), 243–251. DOI 10.1016/0048-9697(96)05179-0.
14. Zhai, W. W., Dai, Y. X., Zhao, W. L., Yuan, H. H., Qiu, D. S. et al. (2020). Simultaneous immobilization of the cadmium, lead and arsenic in paddy soils amended with titanium gypsum. *Environmental Pollution*, 258, 113790. DOI 10.1016/j.envpol.2019.113790.
15. Da, Y., He, T., Shi, C., Lin, Y. (2021). Utilizing titanium-containing pickling sludge to prepare raw meal for clinker production. *Construction and Building Materials*, 268, 121216. DOI 10.1016/j.conbuildmat.2020.121216.
16. Yessengaziyev, A., Ultarakova, A., Kenzhaliyev, B., Burns, P. C. (2019). Research of the leaching process of industrial waste of titanium production with nitric acid. *Journal of Chemical Technology & Metallurgy*, 54(5), 1061–1071.
17. Gazquez, M. J., Bolivar, J. P., Vaca, F., García-Tenorio, R., Caparros, A. (2013). Evaluation of the use of TiO₂ industry red gypsum waste in cement production. *Cement and Concrete Composites*, 37, 76–81. DOI 10.1016/j.cemconcomp.2012.12.003.

18. Gázquez, M. J., Bolívar, J. P., Vaca, F., García-Tenorio, R., Mena-Nieto, A. (2012). Use of the red gypsum industrial waste as substitute of natural gypsum for commercial cements manufacturing. *Materiales de Construcción*, 62(306), 183–198.
19. Zhang, J. F., Yan, Y., Hu, Z. Y. (2018). Preparation and characterization of foamed concrete with Ti-extracted residues and red gypsum. *Construction and Building Materials*, 171, 109–119. DOI 10.1016/j.conbuildmat.2018.03.072.
20. Zhang, J. F., Yan, Y., Hu, Z. Y., Xie, X. L., Yang, L. (2019). Properties and hydration behavior of Ti-extracted residues-red gypsum based cementitious materials. *Construction and Building Materials*, 218, 610–617. DOI 10.1016/j.conbuildmat.2019.05.099.
21. Cai, Q., Ma, B., Jiang, J., Wang, J. Q., Shao, Z. Y. et al. (2021). Utilization of waste red gypsum in autoclaved aerated concrete preparation. *Construction and Building Materials*, 291, 123376. DOI 10.1016/j.conbuildmat.2021.123376.
22. Zhang, Y. H., Wang, F., Huang, H. W., Guo, Y. X., Li, B. Y. et al. (2016). Gypsum blocks produced from TiO₂ production by-products. *Environmental Technology*, 37(9), 1094–1100. DOI 10.1080/09593330.2015.1102329.
23. Hughes, P. N., Glendinning, S., Manning, D. A. C., Noble, B. C. (2010). Production of ‘green’ concrete using red gypsum and waste. *Proceedings of the Institution of Civil Engineers-Engineering Sustainability*, 163(3), 137–146. DOI 10.1680/ensu.2010.163.3.137.
24. Clark, B. A., Brown, P. W. (1999). The formation of calcium sulfoaluminate hydrate compounds: Part I. *Cement and Concrete Research*, 29(12), 1943–1948. DOI 10.1016/S0008-8846(99)00200-8.
25. Clark, B. A., Brown, P. W. (2000). The formation of calcium sulfoaluminate hydrate compounds: Part II. *Cement and Concrete Research*, 30(2), 233–240. DOI 10.1016/S0008-8846(99)00234-3.
26. Li, Y., Qiao, C. Y., Ni, W. (2020). Green concrete with ground granulated blast-furnace slag activated by desulfurization gypsum and electric arc furnace reducing slag. *Journal of Cleaner Production*, 269, 122212. DOI 10.1016/j.jclepro.2020.122212.
27. Schöler, A., Lothenbach, B., Winnefeld, F., Zajac, M. (2015). Hydration of quaternary Portland cement blends containing blast-furnace slag, siliceous fly ash and limestone powder. *Cement and Concrete Composites*, 55, 374–382. DOI 10.1016/j.cemconcomp.2014.10.001.
28. Duan, S. Y., Liao, H. Q., Cheng, F. Q., Song, H. P., Yang, H. Q. (2018). Investigation into the synergistic effects in hydrated gelling systems containing fly ash, desulfurization gypsum and steel slag. *Construction and Building Materials*, 187, 1113–1120. DOI 10.1016/j.conbuildmat.2018.07.241.
29. Huang, Z. Q., Yilmaz, E., Cao, S. (2021). Analysis of strength and microstructural characteristics of mine backfills containing fly ash and desulfurized gypsum. *Minerals*, 11(4), 409. DOI 10.3390/min11040409.
30. Yan, J. Y., Song, Y. M., Wang, Z. J., Wang, B., Xu, H. Z. (2016). Effect of Ca/Si ratio on the properties of autoclaved concrete containing CFBC fly ash. *Materials Reports*, 30(S1), 416–419+423.
31. Schulte Holthausen, R., Raupach, M. (2021). Influence of fresh concrete pressure on cover porosity investigated by single-sided proton nuclear magnetic resonance. *Magazine of Concrete Research*, 73(1), 45–54. DOI 10.1680/jmacr.18.00495.
32. Zhao, H. T., Ding, J., Huang, Y. Y., Tang, Y. M., Xu, W. et al. (2019). Experimental analysis on the relationship between pore structure and capillary water absorption characteristics of cement-based materials. *Structural Concrete*, 20(5), 1750–1762. DOI 10.1002/suco.201900184.
33. Wang, X. X., Shen, X. D., Wang, H. L., Gao, C., Zhang, T. (2016). Nuclear magnetic resonance analysis of freeze-thaw damage in natural pumice concrete. *Materiales de Construcción*, 66(322), e087. DOI 10.3989/mc.2016.09014.
34. Zhang, J. X., Jin, S. S. (2014). *Microscopic pore structure of cement concrete and its function*. Beijing: Science Press.
35. Mehta, P. K. (1986). Hardened cement paste-microstructure and its relationship to properties. *Proceedings of 8th International Congress on the Chemistry of Cement*, vol. I, pp. 113–121. Rio de Janeiro, Fined.
36. Wang, C., Liu, Z. L., Yu, L. (2018). Relationship between anti-frozen durability and pore structure on concrete in freeze and thaw cycle environment. *MATEC Web of Conferences*, 238, 02010. Anshan, China, EDP Sciences. <https://doi.org/10.1051/mateconf/201823802010>.